crystals

MDPI

Article

Laser Terahertz Emission Microscope for Imaging Grain Heterogeneity: A Case Study of $CH_3NH_3PbI_3$ Perovskite Semiconductors

Zhaoyu Liu [1,2], Liang Luo [1], Joongmok Park [1,2], Richard H. J. Kim [1], Zhaoning Song [3], Deniz Turan [4], Mona Jarrahi [4], Yanfa Yan [3] and Jigang Wang [1,2,*]

1 Ames National Laboratory-USDOE, Ames, IA 50011, USA
2 Department of Physics and Astronomy, Iowa State University, Ames, IA 50011, USA
3 Department of Physics and Astronomy and Wright Center for Photovoltaics Innovation and Commercialization, The University of Toledo, Toledo, OH 43606, USA
4 Electrical and Computer Engineering, University of California–Los Angeles, Los Angeles, CA 90095, USA
* Correspondence: jgwang@iastate.edu

Abstract: Strong terahertz (THz) emission from the methylammonium lead iodide ($MAPbI_3$) perovskite semiconductors has been observed following above-bandgap photoexcitation, yet local THz responses of crystalline microstructures are absent. We implement laser THz emission microscope (LTEM), yet-to-be applied to the perovskite semiconductors, as a novel and complementary tool to evaluate the electronic and grain heterogeneity of $MAPbI_3$ thin films. Two $MAPbI_3$ samples with different grain sizes are studied. Using this approach, we show that the one with a larger grain size gives more uniform THz radiation. More significant spatial THz intensity fluctuation is observed for the sample with a smaller grain size.

Keywords: laser terahertz emission microscope; perovskite; terahertz imaging

check for updates

Citation: Liu, Z.; Luo, L.; Park, J.; Kim, R.H.J.; Song, Z.; Turan, D.; Jarrahi, M.; Yan, Y.; Wang, J. Laser Terahertz Emission Microscope for Imaging Grain Heterogeneity: A Case Study of $CH_3NH_3PbI_3$ Perovskite Semiconductors. *Crystals* **2022**, *12*, 1462. https://doi.org/10.3390/cryst12101462

Academic Editor: Younes Hanifehpour

Received: 22 September 2022
Accepted: 9 October 2022
Published: 17 October 2022

Publisher's Note: MDPI stays neutral with regard to jurisdictional claims in published maps and institutional affiliations.

Copyright: © 2022 by the authors. Licensee MDPI, Basel, Switzerland. This article is an open access article distributed under the terms and conditions of the Creative Commons Attribution (CC BY) license (https://creativecommons.org/licenses/by/4.0/).

1. Introduction

Organic-inorganic hybrid lead halide perovskite is one of the promising candidates for next-generation solar cells due to its advantages, such as low-cost manufacturing process and high photoconversion efficiency, which has attracted significant research attention over the past few years [1–5]. As the prototype perovskite material, methylammonium lead iodide ($MAPbI_3$) shows excellent photophysical properties, such as strong absorption in the visible range and extremely long carrier diffusion length [6,7]. In addition to solar cell applications, perovskites have been demonstrated as other optoelectronic devices, such as lasers [8] and light-emitting diodes (LEDs) [9]. Recent research interest extends to the potential application in THz emission [10–12]. When a perovskite thin film is photoexcited by an ultrafast pulse above the bandgap, the emerging transient current generated on a picosecond (ps) time scale leads to the free-space THz emission [13,14]. The strong THz emission from $MAPbI_3$ thin film at room temperature has been observed by several studies [10–12]. Possible mechanisms, such as photo-Dember, lateral photo-Dember [10], and surface depletion fields due to defects [11], have been proposed to explain the generation of THz radiation in $MAPbI_3$ thin films. The reported highest electric field of THz emission from $MAPbI_3$ thin film is one order of magnitude lower than the efficient THz emitter of p-type InAs [11].

Laser THz emission microscopy (LTEM) is a THz imaging technique that reflects the spatial variations of THz emission intensity of a thin film after photoexcitation by an ultrafast laser pulse. The most pronounced advantage of LTEM compared to other THz spectroscopy is the much-improved spatial resolution. In the LTEM, the spatial resolution is limited by the focused excitation beam size rather than emitted THz wavelength; therefore, the resolution can be sub-μm. The LTEM scheme measures photocurrent transport that

complements conventional PL measurements for carrier density and recombination in photovoltaic research. The physics mechanisms of the two methods are different. As a novel characterization tool, LTEM has been demonstrated in potential applications, such as semiconductor device inspection [15] and polycrystalline silicon solar cell evaluation [16]. However, LTEM has never been applied to metal halide perovskite materials, in contrast to PL, which has been extensively used. Inspired by $MAPbI_3$'s strong THz radiation under photoexcitation, it is possible to apply the LTEM to characterize the quality of perovskite thin film samples.

In this letter, we report the imaging of the THz emission from two $MAPbI_3$ perovskite thin film samples with different grain sizes at room temperature by employing a custom-built LTEM setup. The $MAPbI_3$ thin films with and without 5% lead thiocyanate ($Pb(SCN)_2$) additive were prepared on soda-lime glass substrates following a one-step solution process [17] and capped by a 30 nm polymethyl methacrylate (PMMA) protection layer. The spatial homogeneity of THz emission intensity varies with the sample quality. The sample with stronger photoluminescence (PL) signal and larger grain size shows more uniform THz radiation. In addition, the excitation angle dependent THz emission measurements reveal that the transient photocurrent direction is normal to the sample surface.

2. Materials and Methods

The experimental setup is illustrated in Figure 1a. A noncollinear optical parametric amplifier (NOPA) centered at 800 nm with 22 fs pulse width and 2 MHz repetition rate is frequency-doubled by a beta barium borate (BBO) crystal. Then, the horizontally-polarized 400 nm pulse is focused on the perovskite thin film sample by a 50× long working distance objective with a 0.9 μm focal spot size. The excitation power of the 400 nm pulse is 6 mW. A two-dimensional (2D) piezo XY scanner is used to raster scan the sample in order to map out 2D images. The radiated THz electric field in transmission geometry is collected and focused onto a photoconductive THz detector with a bandwidth up to 4.5 THz [18]. An optical delay stage is used to control the relative delay between a heterodyning optical beam and the received THz radiation. The THz emission intensity as a function of photoexcitation angle is measured by rotating the sample orientation. During the measurement, the setup was purged with nitrogen gas to minimize the sample degradation and THz absorption by moisture. The substrates were placed to face the excitation beam. Further experimental details for THz spectroscopy [19–23] and other THz microscopy [24,25] can be found elsewhere.

PL measurements have been adapted as a standard and well-accepted method to inspect the quality of perovskite thin films [26,27]. Higher PL intensity and longer decay lifetimes are indicators of better functional materials [26]. To demonstrate the quality of samples used in the experiment, we performed PL image measurements using our home-built confocal scanning microscope [5]. The resolution of the confocal scanning microscope image system is ∼0.5 μm under 400 nm excitation. The corresponding two 5 μm × 5 μm PL images of $MAPbI_3$ thin films with and without $Pb(SCN)_2$ additives are shown in Figure 1b,c, respectively, at an excitation fluence close to one sun (100 mW/cm^2). The PL image of $MAPbI_3$ thin film with $Pb(SCN)_2$ in Figure 1b shows bright and large grain size (>1 μm). The grain interior and grain boundary can be clearly distinguished with higher PL counts inside the grain. On the contrary, the PL image of $MAPbI_3$ without $Pb(SCN)_2$ shows much weaker PL emission, as in Figure 1c, in which no clear grain/grain boundary structure can be resolved. The larger bright region is a cluster of signals from multi small grains. The grain size is much smaller than our resolution, and one cannot tell them apart. The grain size observed from PL measurement is consistent with the previously reported scanning electron microscope (SEM) images where the grain size of the $MAPbI_3$ thin film with $Pb(SCN)_2$ additive is ∼2 μm and the one without an additive is ∼100–400 nm [17]. Through PL measurement, we confirmed the $MAPbI_3$ with $Pb(SCN)_2$ additive used in the experiment is of higher quality than the one without $Pb(SCN)_2$ additive.

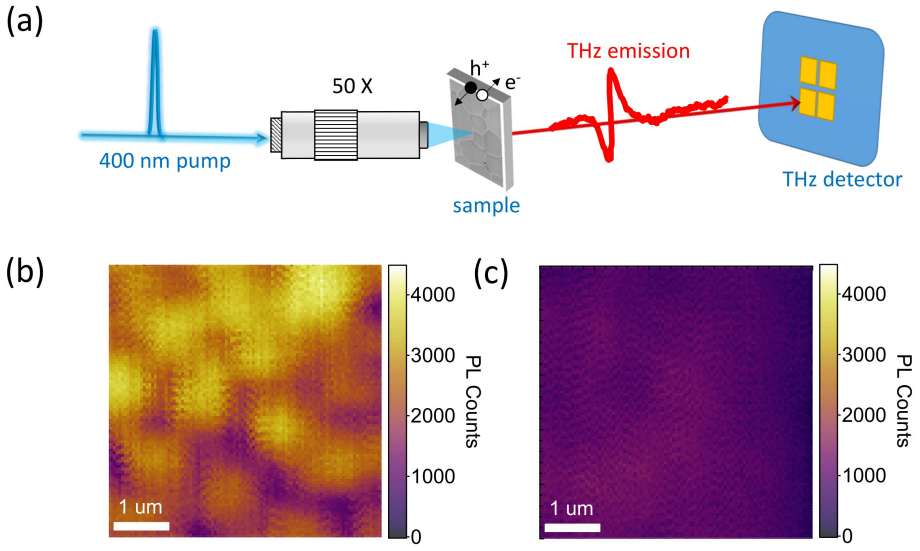

Figure 1. (**a**) Schematic illustration of the LTEM setup in transmission geometry. The photoexcited charges move in the direction perpendicular the sample surface as to be discussed later. PL images of $MAPbI_3$ perovskite thin film sample with (**b**) and without (**c**) $Pb(SCN)_2$ additives at room temperature. The scale bar is 1 μm.

3. Results

In Figure 2, we performed LTEM on $MAPbI_3$ thin films with and without $Pb(SCN)_2$ additive. The THz emission 2D images were plotted as the peak amplitude of THz radiation by fixing the time delay at ~3.5 ps, as shown in Figure 3a. The photoexcitation angle was set at 45 degrees for a larger THz signal size, to be discussed in Figure 3. The image scan range here is 2.5 μm × 5 μm with 100 nm step size and 2 s pixel dwell time. The THz emission images clearly reflect the difference between the two samples. From the previous report [17] and our PL measurement in Figure 1, the $MAPbI_3$ sample with $Pb(SCN)_2$ additive has a larger grain size than the one without it. The THz emission image from $MAPbI_3$ sample with $Pb(SCN)_2$ additive in Figure 2a shows a much smaller spatial fluctuation than the one without the $Pb(SCN)_2$ additive (Figure 2b). Figure 2c compares spatial variation within the selected areas as labeled by the dashed rectangular box in Figure 2a,b. The positions of the rectangular boxes are selected based on the area where the largest THz fluctuation has been observed for the proof of principle demonstration of the technique. It is clearly visible that the spatial fluctuation of THz peak amplitude from the sample without $Pb(SCN)_2$ additive is more than three times larger than the sample with the additive. The data show that a larger grain size results in more uniform THz emission. By adding $Pb(SCN)_2$ additive, the perovskite sample will enable the passivation of grain boundary [17]. The significant spatial variation in the $MAPbI_3$ without $Pb(SCN)_2$ additive indicates that the grain boundary may play a detrimental role in the THz emission. From PL images and LTEM images, the sample with a larger grain size exhibits both stronger PL emission and more uniform THz radiation. Therefore, in addition to conventional PL microscopy, the LTEM can also be used to inspect the quality of perovskite samples.

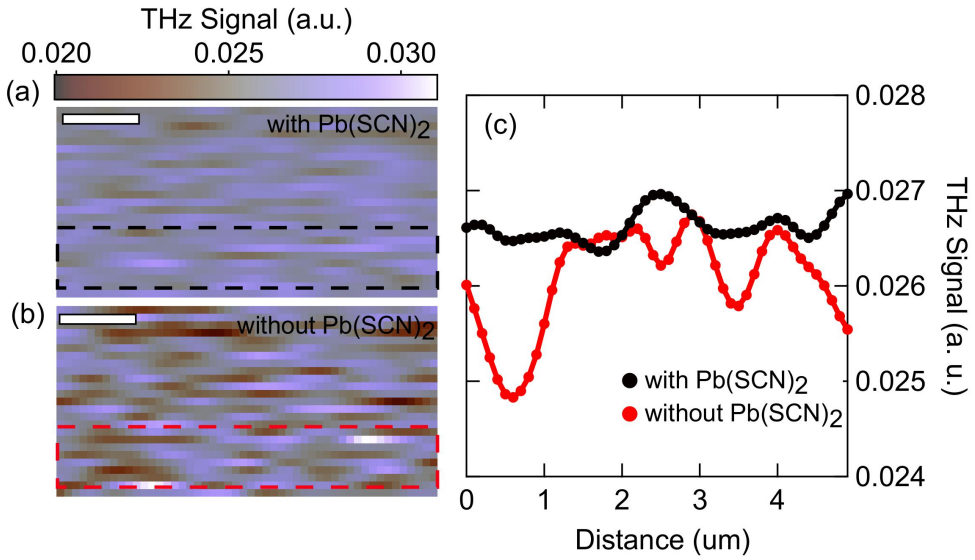

Figure 2. LTEM 2D images of $MAPbI_3$ perovskite thin film samples with (**a**) and without (**b**) $Pb(SCN)_2$ additives upon excitation with 400 nm laser pulse at the power of 6 mW and 45 degree incident angle at room temperature; (**c**) local spatial fluctuation of THz emission peak amplitude from perovskite samples with (black) and without (red) $Pb(SCN)_2$ additives as indicated by the black (**a**) and red (**b**) dashed rectangular box.

Figure 3a shows a typical time-domain THz emission signal from the $MAPbI_3$ thin film sample with $Pb(SCN)_2$ additive and 400 nm excitation at room temperature. Note the emitted THz amplitude is independent of the excitation laser polarization [10]. The corresponding frequency domain spectrum is shown in Figure 3b. Unlike the reflection geometry measurement, which shows multiple peaks between 0–3 THz [10,11], the THz emission spectrum from the transmission geometry shows a single broad peak centered at ~0.3 THz. This might be related to the strong THz absorption in a 1–3 THz range [28].

In the end, we show the effect of excitation angle on the detected THz amplitude. We measured the THz radiation on the $MAPbI_3$ thin film with $Pb(SCN)_2$ additive at 0, 30, and 45 degree excitation angles by rotating the sample. The excitation angle θ is defined as the angle between the incident beam and the normal direction to the sample surface (inset of Figure 3a). As shown in Figure 3c, the strongest THz radiation signal is observed at a 45 degree excitation angle. As the excitation angle becomes smaller, the amplitude of measured THz signal is reduced. The THz signal is negligible under normal incident excitation $\theta = 0$. The excitation angle dependent measurement indicates that the emitted THz is generated by a transient photocurrent in the direction normal to the sample surface [29]. For this reason, the excitation angle was set at 45 degrees for LTEM 2D images presented in Figure 2.

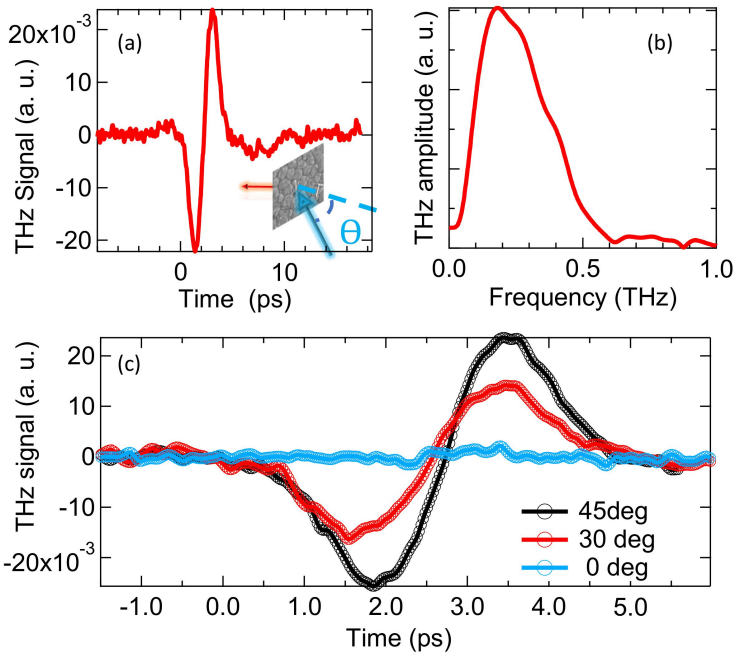

Figure 3. (**a**) Time−domain THz electric field emitted by $MAPbI_3$ thin film sample with $Pb(SCN)_2$ additive; (**b**) the corresponding Fourier spectrum of the emitted THz field exhibiting a main broad peak centered at ∼0.3 THz; (**c**) THz emission signal at a few excitation angles θ (illustrated in the inset of (**a**)) relative to the normal to the sample.

4. Conclusions

In conclusion, we reveal THz emission from the photoexcited transient current on $MAPbI_3$ thin film samples with and without the $Pb(SCN)_2$ additive. The photocurrent direction is normal to the sample surface. The corresponding THz emission 2D images of the two samples are obtained by LTEM. Sample grain size closely correlates with the spatial THz emission homogeneity. For perovskite samples with a larger grain size, the local THz emission fluctuation is smaller. Therefore, LTEM has shown great potential as a novel tool to inspect and characterize the $MAPbI_3$ sample quality.

Author Contributions: Conceptualization, J.W.; software, J.P.; formal analysis, Z.L., J.W.; resources, R.H.J.K., Z.S., Y.Y., D.T. and M.J.; writing—original draft preparation, Z.L.; writing—review and editing, L.L., J.W.; supervision, J.W. All authors have read and agreed to the published version of the manuscript.

Funding: This work was supported by the Ames National Laboratory, the US Department of Energy, Office of Science, Basic Energy Sciences, Materials Science and Engineering Division under contract #DE-AC02-07CH11358 (THz photocurrent measurement and theory). The THz Instrument was supported in part by the National Science Foundation Award No. 1611454. Jarrahi's group was supported by the Department of Energy (grant # DE-SC0016925). Sample development at the University of Toledo was supported by the National Science Foundation DMR 1400432.

Institutional Review Board Statement: Not applicable.

Informed Consent Statement: Not applicable.

Data Availability Statement: The data presented in this study are available on request from the corresponding author.

Conflicts of Interest: The authors declare no conflict of interest.

Abbreviations

The following abbreviations are used in this manuscript:

THz	terahertz
$MAPbI_3$	methylammonium lead iodide
LTEM	laser THz emission microscope
LED	light-emitting diode
ps	picosecond
fs	femtosecond
PMMA	polymethyl methacrylate
PL	photoluminescence
NOPA	noncollinear optical parametric amplifier
BBO	beta barium borate
SEM	scanning electron microscope

References

1. Liu, Z.; Vaswani, C.; Yang, X.; Zhao, X.; Yao, Y.; Song, Z.; Cheng, D.; Shi, Y.; Luo, L.; Mudiyanselage, D.-H.; et al. Ultrafast Control of Excitonic Rashba Fine Structure by Phonon Coherence in the Metal Halide Perovskite $CH_3NH_3PbI_3$. *Phy. Rev. Lett.* **2020**, *124*, 157401. [CrossRef] [PubMed]
2. Liu, Z.; Vaswani, C.; Luo, L.; Cheng, D.; Yang, X.; Zhao, X.; Yao, Y.; Song, Z.; Brenes, R.; Kim, R.J.H.; et al. Coherent band-edge oscillations and dynamic longitudinal-optical phonon mode splitting as evidence for polarons in perovskites. *Phys. Rev. B* **2020**, *101*, 115125. [CrossRef]
3. Cheng, D.; Liu, Z.; Luo, L.; Vaswani, C.; Park, J.-M.; Yao, Y.; Song, Z.; Huang, C.; Mudiyanselage, D.-H.; Kim, R.H.J.; et al. Helicity-dependent terahertz photocurrent and phonon dynamics in hybrid metal halide perovskites. *J. Chem. Phys.* **2019**, *151*, 244706. [CrossRef] [PubMed]
4. Luo, L.; Men, L.; Liu, Z.; Mudryk, Y.; Zhao, X.; Yao, Y.; Park, J.-M.; Shinar, R.; Shinar, J.; Ho, K.-M.; et al. Ultrafast terahertz snapshots of excitonic Rydberg states and electronic coherence in an organometal halide perovskite. *Nat. Commun.* **2017**, *8*, 15565. [CrossRef] [PubMed]
5. Liu, Z.; Bhamu, K.C.; Luo, L.; Shah, S.; Park, J.-M.; Cheng, D.; Long, M.; Biswas, R.; Fungara, F.; Shinar, R.; et al. Spatial–temporal spectroscopy characterizations and electronic structure of methylammonium perovskites. *MRS Commun.* **2018**, *8*, 961. [CrossRef]
6. Dong, Q.; Fang, Y.; Mulligan, P.; Qiu, J.; Cao, L.; Huang, J. Electron-hole diffusion lengths > 175 μm in solution-grown $CH_3NH_3PbI_3$ single crystals. *Science* **2015**, *347*, 967–970. [CrossRef]
7. Stranks, S.D.; Eperon, G.E.; Grancini, G.; Menelaou, C.; Alcocer, M.J.P.; Leijtens, T.; Herz, L.M.; Petrozza, A.; Snaith, H.J. Electron-Hole Diffusion Lengths Exceeding 1 Micrometer in an Organometal Trihalide Perovskite Absorber. *Science* **2013**, *342*, 341–344. [CrossRef]
8. Xing, G.; Mathews, N.; Lim, S.S.; Yantara, N.; Liu, X.; Sabba, D.; Grätzel, M.; Mhaisalkar, S.; Sum, T.C. Low-temperature solution-processed wavelength-tunable perovskites for lasing. *Nat. Mater.* **2014**, *13*, 476–480. [CrossRef]
9. Fu, Y.; Zhu, H.; Chen, J.; Hautzinger, M.P.; Zhu, X.-Y.; Jin, S. Metal halide perovskite nanostructures for optoelectronic applications and the study of physical properties. *Nat. Rev. Mater.* **2019**, *4*, 169–188. [CrossRef]
10. Guzelturk, B.; Belisle, R.A.; Smith, M.D.; Bruening, K.; Prasanna, R.; Yuan, Y.; Gopalan, V.; Tassone, C.J.; Karunadasa, H.I.; McGehee, M.D.; et al. Terahertz Emission from Hybrid Perovskites Driven by Ultrafast Charge Separation and Strong Electron–Phonon Coupling. *Adv. Mater.* **2018**, *30*, 1704737. [CrossRef]
11. Ponseca, C.S., Jr.; Arlauskas, A.; Yu, H.; Wang, F.; Nevinskas, I.; Dūda, E.; Vaicăitis, V.; Eriksson, J.; Bergqvist, J.; Liu, X.-K.; et al. Pulsed Terahertz Emission from Solution-Processed Lead Iodide Perovskite Films. *ACS Photonics* **2019**, *6*, 1175. [CrossRef]
12. Obraztsov, P.A.; Lyashenko, D.; Chizhov, P.A.; Konishi, K.; Nemoto, N.; Kuwata-Gonokami, M.; Welch, E.; Obraztsov, A.N.; Zakhidov, A. Ultrafast zero-bias photocurrent and terahertz emission in hybrid perovskites. *Commun. Phys.* **2018**, *1*, 14. [CrossRef]
13. Cong, K.; Vetter, E.; Yan, L.; Li, Y.; Zhang, Q.; Xiong, Y.; Qu, H.; Schaller, R.D.; Hoffmann, A.; Kemper, A.F.; et al. Coherent control of asymmetric spintronic terahertz emission from two-dimensional hybrid metal halides. *Nat. Commun.* **2021**, *12*, 5744. [CrossRef] [PubMed]
14. Luo, L.; Cheng, D.; Song, B.; Wang, L.-L.; Vaswani, C.; Lozano, P.M.; Gu, G.; Huang, C.; Kim, R.H.J.; Liu, Z.; et al. A light-induced phononic symmetry switch and giant dissipationless topological photocurrent in $ZrTe_5$. *Nat. Mater.* **2021**, *20*, 329–334. [CrossRef]
15. Yamashita, M.; Kawase, K.; Otani, C.; Kiwa, T.; Tonouchi, M. Imaging of large-scale integrated circuits using laser terahertz emission microscopy. *Opt. Express* **2005**, *13*, 115–120. [CrossRef]
16. Nakanishi, H.; Fujiwara, S.; Takayama, K.; Kawayama, I.; Murakami, H.; Tonouchi, M. Imaging of a Polycrystalline Silicon Solar Cell Using a Laser Terahertz Emission Microscope. *Appl. Phys. Express* **2012**, *5*, 112301. [CrossRef]
17. Ke, W.; Xiao, C.; Wang, C.; Saparov, B.; Duan, H.-S.; Zhao, D.; Xiao, Z.; Schulz, P.; Harvey, S.P.; Liao, W.; et al. Employing Lead Thiocyanate Additive to Reduce the Hysteresis and Boost the Fill Factor of Planar Perovskite Solar Cells. *Adv. Mater.* **2016**, *28*, 5214. [CrossRef] [PubMed]

18. Yardimci, N.T.; Turan, D.; Cakmakyapan, S.; Jarrahi, M. A high-responsivity and broadband photoconductive terahertz detector based on a plasmonic nanocavity. *Appl. Phys. Lett.* **2018**, *113*, 251102. [CrossRef]
19. Yang, X.; Luo, L.; Vaswani, C.; Zhao, X.; Yao, Y.; Cheng, D.; Liu, Z.; Kim, R.H.J.; Liu, X.; Dobrowolska-Furdyna, M.; et al. Light control of surface-bulk coupling by terahertz vibrational coherence in a topological insulator. *NPJ Quantum Mater.* **2020**, *5*, 13. [CrossRef]
20. Vaswani, C.; Kang, J.H.; Mootz, M.; Luo, L.; Yang, X.; Sundahl, C.; Cheng, D.; Huang, C.; Kim, R.H.J.; Liu, Z.; et al. Light quantum control of persisting Higgs modes in iron-based superconductors. *Nat. Commun.* **2021**, *12*, 258. [CrossRef]
21. Yang, X.; Zhao, X.; Vaswani, C.; Sundahl, C.; Song, B.; Yao, Y.; Cheng, D.; Liu, Z.; Orth, P.P.; Mootz, M.; et al. Ultrafast nonthermal terahertz electrodynamics and possible quantum energy transfer in the Nb_3Sn superconductor. *Phys. Rev. B* **2019**, *99*, 094504. [CrossRef]
22. Luo, L.; Mootz, M.; Kang, J.H.; Huang, C.; Eom, K.; Lee, J.W.; Vaswani, C.; Collantes, Y.G.; Hellstrom, E.E.; Perakis, I.E.; et al. Quantum Coherence Tomography of Lightwave Controlled Superconductivity. *arXiv* **2022**, arXiv:2207.05958.
23. Luo, L.; Yang, X.; Liu, X.; Liu, Z.; Vaswani, C.; Cheng, D.; Mootz, M.; Zhao, X.; Yao, Y.; Wang, C.-Z.; et al. Ultrafast manipulation of topologically enhanced surface transport driven by mid-infrared and terahertz pulses in Bi_2Se_3. *Nat. Commun.* **2019**, *10*, 607. [CrossRef] [PubMed]
24. Kim, R.H.J.; Huang, C.; Luan, Y.; Wang, L.L.; Liu, Z.; Park, J.M.; Luo, L.; Lozano, P.M.; Gu, G.; Turan, D.; et al. Terahertz Nano-Imaging of Electronic Strip Heterogeneity in a Dirac Semimetal. *ACS Photonics* **2021**, *8*, 1873. [CrossRef]
25. Kim, R.H.J.; Park, J.M.; Haeuser, S.; Huang, C.; Cheng, D.; Koschny, T.; Oh, J.; Kopas, C.; Cansizoglu, H.; Yadavalli, K.; et al. Visualizing heterogeneous dipole fields by terahertz light coupling in individual nano-junctions used in transmon qubits. *arXiv* **2022**, arXiv:2207.05960.
26. De Quilettes, D.W.; Vorpahl, S.M.; Stranks, S.D.; Nagaoka, H.; Eperon, G.E.; Ziffer, M.E.; Snaith, H.J.; Ginger, D.S. Impact of microstructure on local carrier lifetime in perovskite solar cells. *Science* **2015**, *348*, 683–686. [CrossRef] [PubMed]
27. Vrućinić, M.; Matthiesen, C.; Sadhanala, A.; Divitini, G.; Cacovich, S.; Dutton, S.E.; Ducati, C.; Atatüre, M.; Snaith, H.; Friend, R.H.; et al. Local Versus Long-Range Diffusion Effects of Photoexcited States on Radiative Recombination in Organic–Inorganic Lead Halide Perovskites. *Adv. Sci.* **2015**, *2*, 1500136.
28. Sendber, M.; Nayak, P.K.; Egger, D.A.; Beck, S.; Müller, C.; Epding, B.; Kowalsky, W.; Kronik, L.; Snaith, H.J.; Pucci, A.; et al. Optical phonons in methylammonium lead halide perovskites and implications for charge transport. *Mater. Horiz.* **2016**, *3*, 613. [CrossRef]
29. Zhang, X.C.; Auston, D.H. Optoelectronic measurement of semiconductor surfaces and interfaces with femtosecond optics. *J. Appl. Phys.* **1992**, *71*, 326. [CrossRef]